

Calculations of giant magnetoresistance in Fe/Cr trilayers using layer potentials determined from *ab initio* methods

This article has been downloaded from IOPscience. Please scroll down to see the full text article.

2007 J. Phys.: Condens. Matter 19 106210

(<http://iopscience.iop.org/0953-8984/19/10/106210>)

View [the table of contents for this issue](#), or go to the [journal homepage](#) for more

Download details:

IP Address: 129.252.86.83

The article was downloaded on 28/05/2010 at 16:30

Please note that [terms and conditions apply](#).

# Calculations of giant magnetoresistance in Fe/Cr trilayers using layer potentials determined from *ab initio* methods

M Pereiro<sup>1,2,5</sup>, D Baldomir<sup>1,2</sup>, S V Man'kovsky<sup>3</sup>, K Warda<sup>4</sup>, J E Arias<sup>2</sup>,  
L Wojtczak<sup>4</sup> and J Botana<sup>1,2</sup>

<sup>1</sup> Departamento de Física Aplicada, Universidade de Santiago de Compostela,  
Santiago de Compostela E-15782, Spain

<sup>2</sup> Instituto de Investigaciones Tecnológicas, Universidade de Santiago de Compostela,  
Santiago de Compostela E-15782, Spain

<sup>3</sup> Institute for Metal Physics of the National Academy of Sciences of Ukraine, Kiev, Ukraine

<sup>4</sup> Solid State Physics Department, University of Łódź, ulica Pomorska 149/153, 90-236 Łódź,  
Poland

E-mail: [fampl@usc.es](mailto:fampl@usc.es)

Received 9 May 2006, in final form 6 December 2006

Published 16 February 2007

Online at [stacks.iop.org/JPhysCM/19/106210](http://stacks.iop.org/JPhysCM/19/106210)

## Abstract

The *ab initio* full-potential linearized augmented plane-wave method explicitly designed for the slab geometry was employed to elucidate the physical origin of the layer potentials for the trilayers  $n\text{Fe}/3\text{Cr}/n\text{Fe}(001)$ , where  $n$  is the number of Fe monolayers. The thickness of the transition-metal ferromagnet has been ranged from  $n = 1$  up to  $n = 8$  while the spacer thickness was fixed to three monolayers. The calculated potentials were inserted in the Fuchs–Sondheimer formalism in order to calculate the giant magnetoresistance (GMR) ratio. The predicted GMR ratio was compared with the experiment and the oscillatory behaviour of the GMR as a function of the ferromagnetic layer thickness was discussed in the context of the layer potentials. The reported results confirm that the interface monolayers play a dominant role in the intrinsic GMR.

## 1. Introduction

Advances in ultrathin-film fabrication techniques have made possible, only quite recently, the construction of thin magnetic transition-metal layers, separated by very thin non-magnetic layers (spacers), forming superlattices or sandwiches. The Fe/Cr/Fe multilayer system has played a fundamental role because the giant magnetoresistance (GMR) was first discovered on it [1]. Control of the spacer thickness with great accuracy, keeping constant the width of the magnetic layers, has been the main preoccupation of experimentalists for a long time,

<sup>5</sup> Author to whom any correspondence should be addressed.

because this factor is one of the basic conditions for obtaining great values of GMR as well as the coupling constant between the magnetic layers, but the variation of the magnetic layer thickness and its influence on GMR had remained without experimental measurements until quite recently [2, 3]. This fact is understandable because most of these experiments have been guided by the so far existing models in either the quantum-well (QW) [4] or the Ruderman–Kittel–Kasuya–Yosida (RKKY) picture [5]. These models study the oscillatory exchange coupling of the magnetic layers, mediated by the electrons in the spacer, as a function of the spacer thickness with the ferromagnetic layer thickness remaining constant in most of the studied layered structures. However, in this work we focus our attention on the GMR effect produced by the variation of the magnetic layer thickness and surprisingly we have found an oscillating magnetic behaviour of the magnetic layers. The explanation resides more in the presence of QW states than invoking the RKKY-like models, as we will see below.

Nowadays, it is well known that the interface between layers plays a dominant role in the GMR and obviously it depends strongly on the materials of the sample [6]. However, the controversy about whether GMR originates from bulk or interface scattering is still open [7]. This paper will throw some light on this controversy because we calculate the contribution to GMR coming from the bulk and the interface layers. Moreover, we will show that the magnetic properties change as a function of the ferromagnetic layer thickness (FLT) and the contribution to the GMR effect of this system is not negligible as we will prove using the Boltzmann model where the potentials are calculated from the *ab initio* data. Thus, we obtain the density of states (DOS) and energy bands for different FLTs and through them we can calculate the potentials. A remarkable fact is that the former potentials are numerically close to those reported by Hood and Falicov [8, 9] which were chosen without an explicit justification. Thanks to considering the full electronic structure of these materials, we are able to obtain directly the magnetoresistance of these Fe/Cr/Fe samples in a good agreement with the experiment, at least for a certain interval of the ferromagnetic layer thickness [3]. It should be stressed that our *ab initio* calculations and the interpretation through the Boltzmann formalism can give us information about some confusion areas where the mesoscopic concepts play a fundamental role such as in the case of the interface. For systems of reduced dimensions (which in this paper corresponds to a number of iron monolayers (MLs) less than four) the physical magnitudes such as the magnetic moments, conductivity or even the spin change drastically their behaviour, having striking consequences for the magnetoresistance effect, for example a considerable enhancement of the GMR ratio.

In this paper, we investigate the GMR for the layer potentials of Fe/Cr/Fe trilayers determined by means of density functional theory (DFT) calculations as a function of the thickness of the Fe layer. Our study is also restricted to the case of current in plane geometry (CIP). Although the study of GMR versus the spacer thickness is well described in the literature, only a few articles are devoted to the case of a variable ferromagnetic layer. Nevertheless, we have found that the study of this case is more suitable for investigating the intrinsic origin of GMR. In order to show and explain our results we have organized the paper as follows: in section 2 we present the method of calculation. The Fe/Cr/Fe trilayer system is described and the physical origin of the layer potentials is determined according to the DFT calculations. Likewise, a brief description of the effective electron masses is presented in the next subsection. After this, the transport model is introduced in such a way that it allows us to use the data based on DFT calculations, in particular for the relaxation time and the effective mass. The method is developed in order to describe the electronic transport of the Fe/Cr/Fe trilayers in analogy to the evolution of the Co/Cu multilayer conductivity [10]. In section 3 the results of our calculations are discussed and the predictions for GMR properties are reported. Section 4 includes some remarks and a brief summary of the paper.

Thus, the aim of this paper is to describe GMR properties by means of the data obtained within the DFT method and applied to the Fuchs–Sondheimer formalism extended for trilayers.

## 2. Method of calculation and computational details

### 2.1. Self-consistent calculations

*Ab initio* electronic structure calculations were performed within the framework of density functional theory in the local spin density approximation (LSDA). The exchange–correlation potential was used in the form of Vosko *et al* [11]. As reported in [12], the use of LSDA instead of the generalized gradient approximation (GGA) in Fe/Cr trilayers is adequate because GGA improves only the geometry optimization, while the energy calculations (in particular, Fermi energy) are more or less the same. Since we use a fixed geometry and the transport properties depend only on the Fermi energy, it is not necessary at all to use the GGA. The Kohn–Sham equations [13] were solved using the full-potential linearized augmented plane wave (FP-LAPW) method in slab geometry [14, 15]. This method is extremely advantageous for computing the electronic structure of magnetic multilayers, because it was designed to take into account the slab geometry and the interaction between the outermost monolayers of the trilayer system and vacuum. Thus, our method guarantees that all trilayer systems investigated in this work are two-dimensional translational invariants. To our best knowledge, this is the first attempt to account specifically for the slab geometry of layers in contrast with other methodologies where the two-dimensional invariance is achieved by inserting vacuum layers to separate the interaction between the slabs [16]. The valence states were calculated in a scalar-relativistic approximation. A grid of 15  $\mathbf{k}$ -points in an irreducible wedge of the 2D BZ was used during self-consistent field (SCF) cycles and, once converged, a mesh of 45  $\mathbf{k}$ -points was considered to evaluate the final energy. Inside the muffin-tin spheres, basis functions with angular momentum components from 1 up to 8 were included. The charge density and potential within the muffin-tin spheres were expanded into the lattice harmonics with angular momentum from 1 up to 6. More than 60 augmented plane waves per atom were used for the variational basis set.

### 2.2. Fe/Cr/Fe trilayers

Calculations were carried out for the slab consisting of three monolayers of Cr(001) and a variable number of Fe monolayers ( $1 \leq n \leq 8$ ), where  $n$  is the number of Fe monolayers. The Fe layers are intrinsically ferromagnetic and the Cr layers are intrinsically antiferromagnetic (see column 4 of tables 1 and 2). Figure 1 shows the schematic picture of 3 ML Cr in between 5 ML Fe for the bcc crystal orientation (001). We consider the monolayers to be in the  $x$ – $y$  plane and stacked along the  $z$  direction. It is well known that the magnetic properties, DOS, and energy bands depend strongly upon the atomic structures of the thin films. Therefore it is necessary to begin with an optimized structure for the  $\text{Fe}_n/\text{Cr}_3$  system. Nevertheless, no further attempt was made to relax the lattice parameter, i.e. the lattice constant for Fe and Cr was assumed to be Cr bcc bulk-like, that is,  $a_0 = 2.88 \text{ \AA}$ , because we observed small differences in the obtained results when these constants were taken differently.

### 2.3. Layer potentials

The single-band model representation leads to the energies

$$E_{v\sigma}(k) = \frac{1}{2}m_{\sigma}^*(v_{\sigma}(k))^2 + V_{v\sigma} \quad (1)$$

**Table 1.** Computational results for Fe<sub>*n*</sub>/Cr<sub>3</sub> trilayers (*n* = 1–4, 6, 8) along with the layer potentials calculated according to equation (2) and the relaxation times provided by equation (6) with *c* = 8.34 × 10<sup>−5</sup>. The symbol *m* denotes magnetic moment per atom, ρ<sub>*ν*</sub>(ε<sub>F</sub>) is the density of states at the Fermi level and V<sub>*νσ*</sub> represents the potential of the majority and minority spins per monolayer.

Trilayer	E <sub>F</sub> (eV)	ML	<i>m</i> ( $\frac{\mu_B}{\text{at.}}$ )	ρ <sub><i>ν</i></sub> (ε <sub>F</sub> ) (eV <sup>−1</sup> )		V <sub><i>νσ</i></sub> (eV)		τ <sub><i>νσ</i></sub> <sup>*</sup> (10 <sup>−13</sup> s)	
				↑	↓	↑	↓	↑	↓
Fe <sub>1</sub> /Cr <sub>3</sub>	−4.32	Fe(1)	2.45	0.54	3.76	−6.90	−4.90	3.07	0.87
		Cr(1)	−0.62	0.95	0.50	−7.30	−7.30	2.35	1.58
		Cr(2)	0.62	0.63	0.94	−7.30	−7.30	1.56	2.96
Fe <sub>2</sub> /Cr <sub>3</sub>	−3.97	Fe(1)	2.94	0.13	2.88	−8.19	−5.83	9.05	0.81
		Fe(2)	1.94	0.39	0.64	−7.86	−6.14	3.28	3.27
		Cr(1)	−0.47	0.81	0.83	−7.69	−7.69	1.65	1.61
Fe <sub>3</sub> /Cr <sub>3</sub>	−4.32	Cr(2)	0.35	0.33	0.50	−7.69	−7.69	4.04	2.67
		Fe(1)	2.92	0.14	2.12	−8.7	−6.3	7.45	0.94
		Fe(2)	2.43	0.15	0.62	−8.5	−6.4	7.28	3.11
Fe <sub>4</sub> /Cr <sub>3</sub>	−4.32	Fe(3)	2.00	0.32	0.44	−8.3	−6.7	3.58	4.00
		Cr(1)	−0.75	0.53	0.40	−6.3	−6.3	3.75	4.97
		Cr(2)	0.71	0.21	0.23	−6.3	−6.3	4.47	8.65
Fe <sub>6</sub> /Cr <sub>3</sub>	−3.95	Fe(1)	2.97	0.17	2.32	−9.3	−7.3	5.37	0.45
		Fe(2)	2.27	0.28	0.34	−9.3	−7.3	3.26	4.36
		Fe(3)	2.49	0.26	0.57	−9.3	−7.3	3.51	2.60
Fe <sub>8</sub> /Cr <sub>3</sub>	−3.97	Fe(4)	2.16	0.34	0.53	−9.3	−7.3	2.68	2.79
		Cr(1)	−0.50	0.89	0.63	−7.2	−7.2	1.71	2.42
		Cr(2)	0.50	0.25	0.40	−7.2	−7.2	6.09	3.81
Fe <sub>6</sub> /Cr <sub>3</sub>	−3.95	Fe(1)	2.96	0.08	1.72	−9.4	−7.3	11.16	0.86
		Fe(2)	2.25	0.23	0.36	−9.4	−7.3	3.88	4.11
		Fe(3)	2.41	0.38	0.28	−9.4	−7.3	2.35	5.29
Fe <sub>6</sub> /Cr <sub>3</sub>	−3.95	Fe(4)	2.25	0.41	0.34	−9.4	−7.3	2.18	4.36
		Fe(5)	2.34	0.28	0.21	−9.4	−7.3	3.19	7.05
		Fe(6)	2.20	0.26	0.47	−9.4	−7.3	3.44	3.15
Fe <sub>6</sub> /Cr <sub>3</sub>	−3.95	Cr(1)	−0.65	0.49	0.25	−7.6	−7.6	2.79	5.47
		Cr(2)	0.58	0.52	0.48	−7.6	−7.6	2.63	2.85
		Fe(1)	2.98	0.04	1.91	−9.3	−7.3	22.81	0.78
Fe <sub>6</sub> /Cr <sub>3</sub>	−3.95	Fe(2)	2.19	0.14	0.36	−9.3	−7.3	6.52	4.11
		Fe(3)	2.35	0.10	0.44	−9.3	−7.3	9.13	3.37
		Fe(4)	2.19	0.14	0.34	−9.3	−7.3	6.52	4.36
Fe <sub>6</sub> /Cr <sub>3</sub>	−3.95	Fe(5)	2.26	0.13	0.30	−9.3	−7.3	7.02	4.94
		Fe(6)	2.25	0.17	0.39	−9.3	−7.3	5.37	3.80
		Fe(7)	2.35	0.17	0.32	−9.3	−7.3	5.37	4.63
Fe <sub>8</sub> /Cr <sub>3</sub>	−3.97	Fe(8)	2.13	0.36	0.71	−9.3	−7.3	2.54	2.09
		Cr(1)	−0.64	1.01	0.43	−7.7	−7.7	1.32	3.10
		Cr(2)	0.49	0.29	0.46	−7.7	−7.7	4.59	2.89

of electrons moving in the intrinsic potential  $V_{\nu\sigma}$  with the spin  $\sigma$  in monolayer  $\nu$  and velocity  $v_\sigma(k)$ . The intrinsic potentials require for these calculations to be determined on the basis of *ab initio* DFT calculations described in section 2.1. Since these values are the electron energies corresponding to the bottom of the conductivity band, they were taken to be equal to the energies of s, p electrons at the  $\Gamma$ -point of the 2D BZ, since we assume that these electrons

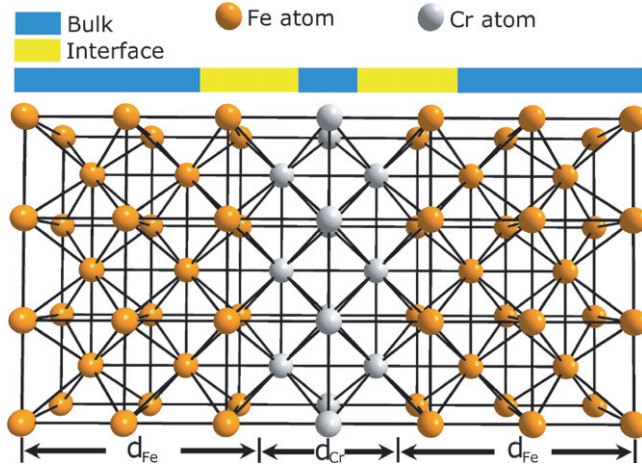


**Figure 1.** Schematic picture of the generic Fe<sub>n</sub>/Cr<sub>3</sub>(001) system. The bulk and interface monolayers are indicated in the figure.

(This figure is in colour only in the electronic version)

**Table 2.** Computational results for Fe<sub>n</sub>/Cr<sub>3</sub> trilayers ( $n = 5, 7$ ) along with the layer potentials calculated according to equation (2) and the relaxation times provided by equation (6) with  $c = 8.34 \times 10^{-5}$ . The symbols are the same as in table 1.

Trilayer	$E_F$ (eV)	ML	$m$ $\left(\frac{\mu_B}{\text{at.}}\right)$	$\rho_\nu(\epsilon_F)$ (eV <sup>-1</sup> )		$V_{\nu\sigma}$ (eV)		$\tau_{\nu\sigma}^*$ (10 <sup>-13</sup> s)	
				↑	↓	↑	↓	↑	↓
Fe <sub>5</sub> /Cr <sub>3</sub>	-4.56	Fe(1)	2.93	0.17	2.50	-9.4	-7.3	5.04	0.61
		Fe(2)	2.35	0.27	0.92	-9.4	-7.3	3.31	1.61
		Fe(3)	2.41	0.39	0.29	-9.4	-7.3	2.29	5.11
		Fe(4)	1.79	0.48	0.79	-9.4	-7.3	1.86	1.88
		Fe(5)	3.12	0.32	0.21	-9.4	-7.3	2.79	7.05
		Cr(1)	-0.94	0.52	0.45	-7.4	-7.4	2.77	3.20
		Cr(2)	0.64	0.20	0.14	-7.4	-7.4	7.21	10.30
Fe <sub>7</sub> /Cr <sub>3</sub>	-4.02	Fe(1)	2.96	0.17	2.70	-9.3	-7.3	5.37	0.55
		Fe(2)	2.24	0.46	0.44	-9.3	-7.3	1.98	3.37
		Fe(3)	2.29	0.47	0.22	-9.3	-7.3	1.94	6.73
		Fe(4)	2.21	0.52	0.37	-9.3	-7.3	1.76	4.00
		Fe(5)	2.27	0.62	0.13	-9.3	-7.3	1.47	11.39
		Fe(6)	1.77	0.55	0.32	-9.3	-7.3	1.66	4.63
		Fe(7)	2.93	0.50	0.14	-9.3	-7.3	1.83	10.58
		Cr(1)	-0.75	0.51	0.25	-7.7	-7.7	2.61	5.32
		Cr(2)	0.50	0.49	0.46	-7.7	-7.7	2.72	2.89

make the main contribution to the conductivity. To describe the spin-dependent conductivity within our model, these energies were split by the value  $\Delta E^{\text{d-band}}$  which is equal to the energy splitting of majority and minority-spin d-bands in Fe layers while in Cr layers the potential values were taken the same for both spin directions. Thus,

$$V_{\nu\sigma} = E_\nu^{\text{s,p-band}}(\mathbf{k} = 0) - \zeta \sigma \Delta E^{\text{d-band}} \quad (2)$$

where  $\zeta = 1$  for the Fe slab and  $\zeta = 0$  for the Cr slab. Note that the spin electron in Bohr magneton units is  $\sigma = +\frac{1}{2}$  for majority electrons and  $\sigma = -\frac{1}{2}$  for minority electrons and the confinement of electrons within two-dimensional slab results in quantization of electron states in the direction perpendicular to the plane of this slab ( $z$ -direction). This quantum-size effect

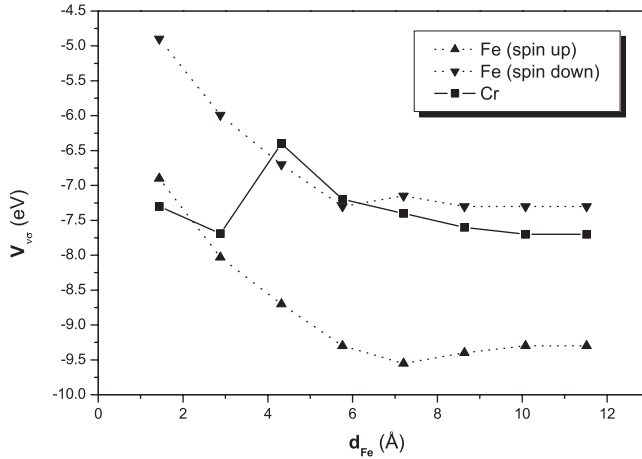


**Figure 2.** Dependence of the Fe majority (triangles), Fe minority (inverted triangles) and Cr (squares) layer potentials versus the FLT,  $d_{\text{Fe}}$ , for a fixed Cr thickness,  $d_{\text{Cr}} = 4.32 \text{ \AA}$ . For  $n \leq 3$ , the values of the layer potentials are given on average.

is essential, especially when the slab thickness is restricted to several atomic layers [17–19]. Therefore, we took it into account in our present calculations when the thickness of the Fe film was equal to one, two or three atomic layers.

Since the quantum-well electronic states, in the case of ultrathin Fe films, are well localized in a single atomic layer, we assume that the physical properties on this layer are determined mainly by the states which have a degree of localization in the layer more than 60%. The energy of the electron state at the  $\Gamma$ -point corresponding to the energy band with high localization in the  $i$ th atomic layer was taken as the  $i$ th potential value. In the case of a thicker Fe film ( $n \geq 4$ ) the electron states are more delocalized and they cannot be related to only one atomic layer, therefore we took in these cases the values of potentials  $V_{v\sigma}$  common for a whole Fe film. The potential values in the Cr film always had the same value for all Cr atomic layers. The variations of the layer potentials for  $n \geq 4$  are expected to be quite small because of the delocalization of the electron states, as is shown in figure 2.

#### 2.4. Description of the effective mass

The effective mass parameter  $m_{\sigma}^*$  can be calculated by means of the standard procedure of DFT applied to the band structure calculations. An example of the complicated spin-dependent band structure provided by our DFT calculations is shown in figure 3 for the  $\text{Fe}_5/\text{Cr}_3$  system. The effective masses have been calculated as the second derivative of the s, p electronic band energy  $E_{\sigma}(k)$  close to the Fermi level with respect to the Fermi wavevector  $k_{\text{F}}$  and evaluated at the  $\Gamma$ -point, according to the following relation

$$\frac{1}{m_{\sigma}^*} = \frac{1}{\hbar^2} \left( \frac{d^2 E_{\sigma}(k)}{dk^2} \right)_{k=k_{\text{F}}} . \quad (3)$$

The energy band close to the Fermi level could always be approximated by a second-order polynomial in all considered systems. This argument is what underpins the parabolic approximation adopted in section 2.3. The numerical evaluation of the effective masses is collected in table 3. We can observe that our calculated effective masses are close to  $4m_{\text{e}}$ , that is the value assumed for the effective mass in Fe and Cr [8, 20]. To the best of our knowledge, no effective masses have been reported for Fe/Cr multilayers. In layered materials, we have only found the effective masses for Cu thin films deposited on the fcc Co film and they are in good agreement with the ones reported in table 3 [21].

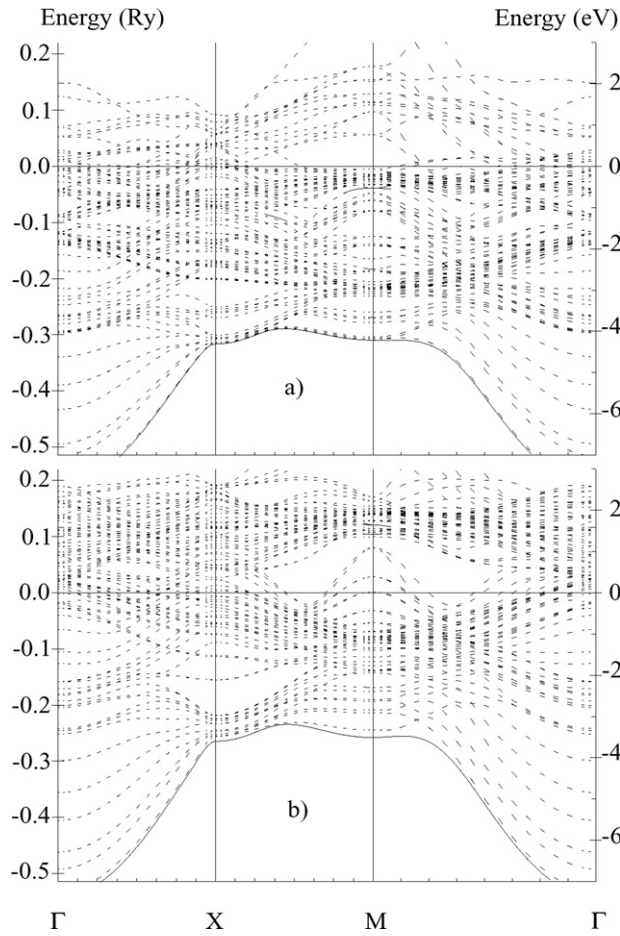


**Figure 3.** Energy bands of the majority-spin states (a) and the minority-spin states (b) for the Fe<sub>5</sub>/Cr<sub>3</sub> system. Solid lines represent the states with more than 50% of localization in the interface Fe layer. The Fermi level is at 0 eV.

**Table 3.** The spin-dependent effective mass parameters in units of the free electron mass ( $m_e$ ).

Trilayer	$m_{\uparrow}^*$ ( $m_e$ )	$m_{\downarrow}^*$ ( $m_e$ )
Fe <sub>1</sub> /Cr <sub>3</sub>	3.15	3.98
Fe <sub>2</sub> /Cr <sub>3</sub>	3.55	4.59
Fe <sub>3</sub> /Cr <sub>3</sub>	3.56	4.62
Fe <sub>4</sub> /Cr <sub>3</sub>	3.85	5.08
Fe <sub>5</sub> /Cr <sub>3</sub>	3.92	5.13
Fe <sub>6</sub> /Cr <sub>3</sub>	3.95	5.17
Fe <sub>7</sub> /Cr <sub>3</sub>	3.93	5.20
Fe <sub>8</sub> /Cr <sub>3</sub>	3.93	5.20

### 2.5. The transport model

In order to consider the transport properties using the DFT data, the electronic transport for the Fe/Cr/Fe trilayers can be described by the Boltzmann formalism [8, 9, 22–25] applied to the current in plane geometry. In every monolayer, the electric current is then determined by appropriate distribution functions in terms of the velocity  $v_z$  in the direction  $z$  perpendicular to



the interface for the electron with spin up and spin down due to the translational symmetry in the plane of the film. The electrons involved in transport are embedded within the potentials  $V_{v\sigma}$  of each monolayer  $v$ . These potentials were determined using the DFT data in conjunction with equation (2).

With the aim of calculating the conductivity we write the Boltzmann equation in the relaxation time  $\tau_{v\sigma}^*$  approximation for the distribution functions  $g_{v\sigma}^\beta$  ( $\beta = +, -$ ) which are determined with respect to the electric field applied in the direction of the electric current. The solutions are found taking into account the boundary conditions at the outer surfaces, namely  $g_{1\sigma}^+ = P_{1\sigma} g_{1\sigma}^-$  (at  $z = 0$ ) and  $g_{n\sigma}^- = P_{n\sigma} g_{n\sigma}^+$  (at  $z = 2(n + 1)a_0$ ) with  $g_{v\sigma}^+$  and  $g_{v\sigma}^-$  standing for the solutions with  $v^z \geq 0$  and  $v^z < 0$ , respectively. In order to extend our considerations to a more realistic case from the physical point of view, we define the specularity factor  $P_{v\sigma}$  on the basis of the physical picture of the electrons involved in transport crossing through the potential barrier. In this case the value of  $P_{v\sigma}$  corresponds to the specularity factor in the Fuchs–Sondheimer [26, 27] conductivity theory of thin films and leads to the effective result

$$P_{v\sigma}(\theta) = \frac{1 - \frac{(\chi_{v\sigma})^2 \cos^4 \theta + 2}{1 + (\chi_{v\sigma})^2 \cos^4 \theta}}{1 - \frac{(\chi_{v\sigma})^2 \cos^4 \theta + 2}{(\chi_{v\sigma})^2 \cos^4 \theta} \exp\left(-\frac{a_0}{\tau_{v\sigma}^* v^2 \cos \theta}\right)} \quad (4)$$

for  $v$  ranging from 1 up to  $2n + 3$ , that is an alternative version to other models which assume the coefficients for coherent transmission and specular reflections determined quantum mechanically by matching free electron wavefunctions and their derivatives at each interface (see figure 1). In equation (4),  $\theta$  is the angle of incidence of electrons measured with respect to the  $z$ -axis. The parameter  $\chi_{v\sigma}$  is defined in terms of the Fermi velocity  $v_F$  as

$$\chi_{v\sigma} = \frac{2m_\sigma^* \tau_{v\sigma}^* v_F^2}{\hbar} \quad (5)$$

where  $m_\sigma^*$  is the effective mass of  $\sigma$  electrons. From the physical point of view  $\chi_{v\sigma}$  represents the ratio of the electron free path with respect to the de Broglie wavelength.

The distribution functions  $g_{v\sigma}^\alpha$  depend on the relaxation times  $\tau_{v\sigma}^*$  which can be evaluated in terms of the DFT calculations by means of the Fermi golden rule. The relaxation time can be expressed as follows [28]:

$$(\tau_{v\sigma}^*)^{-1} = \frac{c}{\hbar} \rho_v(\varepsilon_F) (V_{v\sigma})^2 \quad (6)$$

where  $\rho_v(\varepsilon_F)$  is the local density of states per monolayer  $v$  at the Fermi energy;  $c$  is the number of the scattering centres relative to the total number of atoms and it plays the role of a calibration factor in order to compare it with the average values in the case of samples discussed in the literature. Equation (6) is important for thin films due to the presentation of the relaxation time distribution across a sample.

The total current in CIP geometry along the direction  $\alpha$  defined by the electric field  $\mathbf{E}^\alpha$  is obtained after averaging the current density over the whole thickness of the film and it is given by the relation [8, 9]

$$J^\alpha = \frac{-|e|}{d} \sum_{v=1, \sigma=\uparrow\downarrow}^{2n+3} \left[ \frac{m_\sigma^*}{2\pi\hbar} \right]^3 \int_0^d \int v^\alpha g_{v\sigma}^\beta(\mathbf{v}, z, E^\alpha) d\mathbf{v} dz \quad (7)$$

where  $e$  is the electric charge and  $d$  is the length of the sample in the  $z$  direction. Assuming that the total conductivity of a sample can be defined as  $\Sigma = 1/\rho = (dJ^\alpha/dE)_{E=0}$ , and the magnetoresistance (MR) ratio as  $\Delta\rho/\rho_s = (\rho_{\uparrow\downarrow} - \rho_{\uparrow\uparrow})/\rho_{\uparrow\downarrow}$ , then the theoretical predictions of the GMR can be obtained straightforwardly. It is worth emphasizing that the MR ratio is found by calculating independently the resistivities for the parallel ( $\rho_{\uparrow\uparrow}$ ) and the antiparallel ( $\rho_{\uparrow\downarrow}$ )

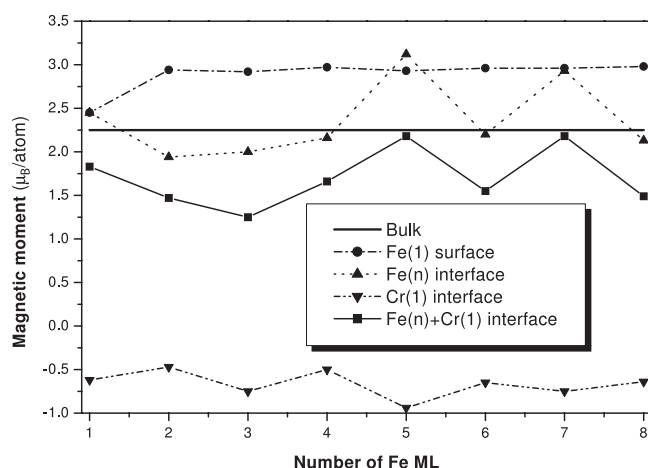


**Figure 4.** Behaviour of the surface (circles) and interface (triangles) Fe magnetic moment versus Fe film thickness. Inverted triangles represent the value of the Cr interface magnetic moment and the squares correspond to the numerical sum of the Fe and Cr interface magnetic moments. The solid line is the magnetic moment of the Fe bulk which is equal to  $2.25 \mu_B$ .

alignment of the magnetic moments in adjacent magnetic layers. The present approach remains in analogy to the calculations of Zahn *et al* [10], who use the semiclassical Boltzmann theory with a spin independent relaxation time approximation. However, in our case, the relaxation time is not only spin dependent but also shows a local character.

Concerning the problem of whether GMR originates from bulk or interface scattering, we consider the contribution to MR from bulk and interface layers separately. An example to allocate the bulk and interface layers where bulk and interface scattering occurs is plotted in figure 1. We have discretized the conductivity layer by layer with appropriate boundary conditions. Thus, the summation of the conductivity of the bulk layers and the conductivity of the interface layers was done independently to obtain the bulk and interface contributions to MR.

### 3. Results and discussion

#### 3.1. Layer magnetic moments and potentials

First, we describe briefly the computational results obtained using the LAPW method. The numerical results of our calculations along with the layer potentials calculated according to equation (2) and the relaxation times provided by equation (6) are presented in tables 1 and 2.<sup>6</sup>

According to figure 4, the behaviour of the magnetic moment versus the Fe film thickness for the interface Fe layer is non-monotonic in contrast with the surface Fe magnetic moment which ranges monotonically from  $2.45 \mu_B$  for  $n = 1$  up to  $2.98 \mu_B$  for  $n = 8$  (see fourth column of tables 1 and 2 for Fe(1) ML). We have also found the existence of highly localized states at the Fe/Cr interface when the Fe film thickness is not too small ( $n \geq 4$ ). These states can result in the onset of a big magnetic moment in the interface Fe layer as also occurs at the

<sup>6</sup> For the sake of notation, a brief comment on tables 1 and 2 is required: Cr(1) stands for the monolayer of Cr that is closest to a Fe monolayer; Cr(2) is the central monolayer of the Cr slab, that is, the second of the three Cr monolayers; Fe(1) stands for the external monolayer of the Fe film; and Fe(2), Fe(3),..., are the corresponding monolayers inside the Fe slab.

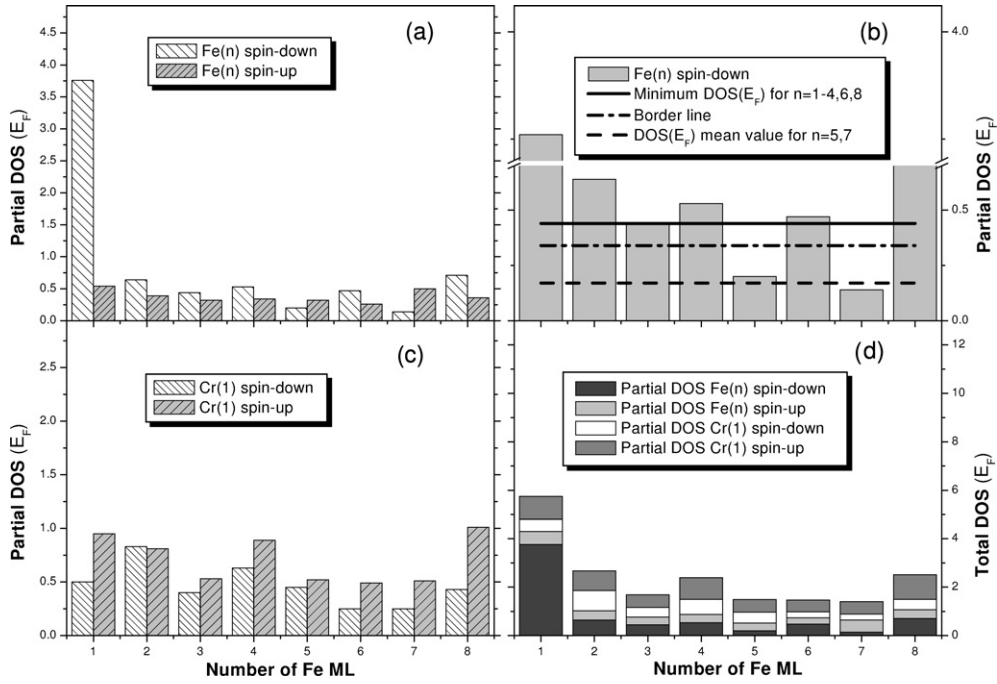


**Figure 5.** Column graph exhibiting the partial DOS ( $\epsilon_F$ ) versus the Fe layer thickness for (a) the Fe interface ML spin-up and down, (b) Fe interface ML spin-down and (c) Cr interface ML spin-up and down polarization. (d) The total DOS ( $\epsilon_F$ ) as a function of the FLT. The dash-dot line in (b) establishes a reasonable criterion for considering the minority spin channels insignificant for the case  $n = 5, 7$ .

surface. However, the localization of these states near the interface means that they should not be affected by the thickness of the Fe film and the magnetic moments near the Fe/Cr interface should be independent of Fe film thickness. This is a feature that, in our opinion, is due to the QW states, which are delocalized throughout the slab and their energy changes together with increase of the Fe film thickness [29]. The QW states have a resonance with the interface states for  $n = 4, 6, 8$ . Consequently, the interface states become less localized, which results in a decrease of their exchange splitting as well as in a decrease of the interface Fe magnetic moment. The opposite behaviour is found for the case  $n = 5, 7$ , leading to an increase of the interface Fe magnetic moment, such as is shown in figure 4.

In this paragraph, our computational results are put in relation with the GMR effect, with the aim of enabling deductions about the effects that enhance the GMR, at least from a qualitative point of view. The quantitative predictions will be shown in section 3.2. For  $n = 5, 7$  we have a special behaviour on the Fe/Cr interface (see table 2), which deserves a more detailed comment. The first characteristic that we obtain, different from what happens for  $n = 1, 2, 3, 4, 6, 8$ , is that we observe that the majority spins are the main contribution at the Fermi level (see figure 5(a)). Notice that the DOS ( $\epsilon_F$ ) minority spin for  $n = 1, 2, 3, 4, 6, 8$  has the corresponding values 3.76, 0.64, 0.44, 0.53, 0.47 and 0.71, while for  $n = 5, 7$  they are 0.21 and 0.14, respectively. As can be inferred, these values are much lower than the previous ones (in figure 5(b), we can see clearly the criterion employed to consider the magnetic channels to be insignificant for  $n = 5, 7$ , where the dash-dot line is the border line between negligible and appreciable channels). In fact, the lowest value for  $n = 1, 2, 3, 4, 6$  and 8 is 0.44, which is

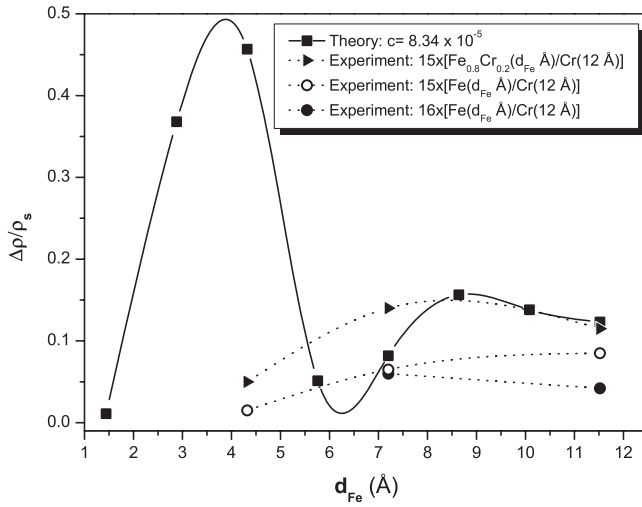


**Figure 6.** Plot of the calculated (solid line) and experimental [3] (dashed lines) MR ratio as a function of the ferromagnetic layer thickness.

above the dash-dot line. Thus, we observe that the minority spin channels are very small for these two special cases in comparison with the ones seen above. The above comments lead us to conclude that our electronic structure calculations within DOS column graphs presented in figure 5 show that there is essentially only one magnetic channel (semimetallic) on the iron–chromium interface for  $n = 5, 7$  (see figures 5(a), (b) and table 2) and a very high increase of the magnetism on its interfaces, since the other channel is the one of the minority spin density, quasiequal to zero. Nevertheless, for  $n = 1, 2, 3, 4, 6$  and  $8$  we obtain both kinds of magnetic polarizations: up and down (see table 1). This situation is very interesting for the GMR effect if we accept that this phenomenon is mainly due to the scattering of the electrons on these interfaces (a feature which will be discussed in section 3.2), that is, the spin-polarized electrons on the one hand enhance their velocity when they find the magnetic polarizability of the impurity parallel to the magnetic layer, but, on the other hand, the spin-polarized electrons diminish their velocity when they find the polarizability in the opposite direction. Therefore, we have a spin valve effect in which there is a selection of one of the two possible magnetic channels, and this drives a decrease or an increase of the conductivity, depending on whether the electrons are parallel or antiparallel to the magnetic polarization of the interface.

### 3.2. GMR predictions

So far, the models based on the Boltzmann equation specially developed for describing the multilayer transport properties introduce the potentials as a parameter or consider them in a semiempirical way [8, 9]. The value of this potential is usually taken as a constant; however, for ultrathin films the potential depends on the thickness of the sample as it was reported in [30] and, consequently, the electronic transport is influenced by the thickness of the sample (not only the thickness of the spacer but also the thickness of the ferromagnetic layer). Contrary to the usual procedure described in the literature, in this paper, the values of the potentials as a function of the FLT were determined using the DFT methods described earlier (see figure 2, tables 1 and 2). The dependence of the MR ratio on the thickness of the ferromagnetic layer  $d_{Fe}$  is shown in figure 6. The values of the MR ratio obtained for the thickness dependent potential are indicated by full rectangles and they were calculated for a dilute concentration of scattering centres, that is, for  $c = 8.34 \times 10^{-5}$  [28]. The calculated MR exhibits an oscillatory behaviour for a thickness in the range of the  $x$  axis displayed by figure 6, although the oscillations appear

at the wrong periodicity compared with the experiments reported in [3]. In the light of the present calculations, we can conclude that the oscillatory character of the GMR comes mainly from a variable potential distribution through out the thin film, since the oscillatory behaviour of the GMR is hidden as long as the potential is allowed to be constant, for example in the case of the semiclassical model in which every layer is represented by a quantum well with a constant potential [8]. The MR ratio shown in figure 6 exhibits two maxima: the first one at around 4 Å and the second one close to 8 Å. Thus, although the period of oscillations is wrong compared to the experiment [3], the second maximum agrees quite well with the measurements and we can observe in figure 6 that the theoretical and experimental values remain in good agreement in the interval of  $d_{\text{Fe}} \geq 8$  Å. Only the proper treatment and choice of the potential allows us to obtain the oscillatory behaviour even in the semiclassical approach [31]. The important problem, which has up till now been omitted in the literature, is the determination of the potential at the interface or even proper treatment of the interface. It is a well known fact that at the interface there exists a significant change of the potential but this change is not of abrupt character. At the interface there is a transition region where the interdiffusion and the spin mixing take place while the change of the potential should be continuous according to the background.

We note that even though on one hand the GMR effect depends strongly on the temperature [32] and on the other hand we are comparing our data (0 K) with the ones reported by Okuno *et al* (77 K) at different temperatures, the influence of the temperature in the interval [0, 77] can be considered negligible [32]. The discrepancy of our results with the experimental ones is less than about 10–15% for  $n \geq 4$ , which represents an improvement with respect to other *ab initio* calculations [33]. The aforementioned small discrepancy may be due to the high number of layers (multilayers) considered in the experiment in comparison with the reduced number of layers (trilayer) of our Fe/Cr sample. For the sake of comparison with the results reported by Okuno *et al*, it is noteworthy that a remarkable message from our results is the low-dependence behaviour of GMR with the number of Fe/Cr layers because the average value of the GMR ratio as a function of the Fe layer thickness is around 0.1 for  $n \geq 4$  in our calculations and in the experimental results. In order to explain this low-dependence behaviour, our proposal consists in considering a quasi-linear dependence of resistance of different numbers of Fe/Cr layers. Thus, after calculating the GMR ratio, the proportional constant is divided by itself, having no appreciable effect in GMR. This tendency disappears for the case of two or three iron monolayers leading to a considerable GMR ratio as shown in figure 6, since the electron states are more localized and, thus, they favour an increase of the layer potentials.

We should remind the reader that studies of transport in metallic superlattices (and particularly for trilayers) are affected by many inherent complexities of the material. Many possible complications arise in these types of artificial material, among them, interfacial interdiffusion at various lateral length scales [34–36], bulk defects, structural changes as a function of an individual layer and overall thicknesses, different length scales affecting the structure, the boundary conditions on the outermost layers and differences in the magnetotransport along the different directions in the superlattices. But the key point in the mechanism of GMR is the relative importance of bulk and interfacial scattering. Measurements as a function of layer thickness have claimed that the GMR originates from the bulk and that the interfacial roughness does not play a crucial role [37, 38] even in the current perpendicular to plane configuration. Other measurements, in which the interface was modified by the addition of small amounts of interfacial impurities, claim that the interfacial scattering plays a dominant role [39]. The bulk and interface contribution to the total MR ratio as a function of the Fe monolayers is shown in figure 7. The results, except for the case  $n = 4$ , clearly show that the monolayers that belong to the interface dominate the GMR because the potential abruptly

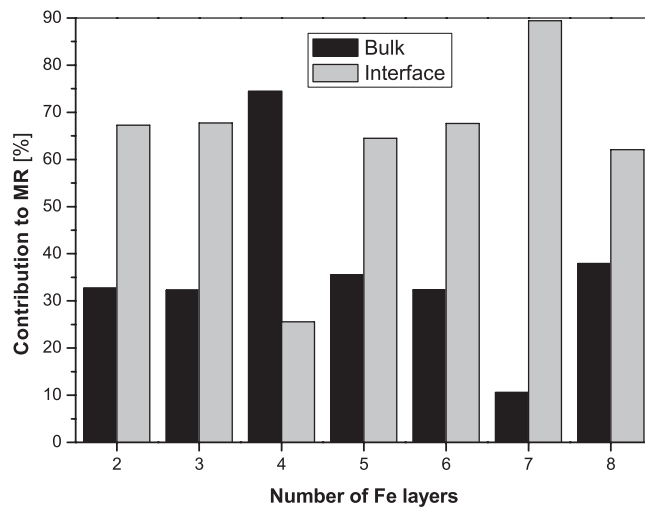


**Figure 7.** Bulk and interface contribution to the total MR ratio versus the thickness of the ferromagnetic layer for  $c = 8.34 \times 10^{-5}$ .

changes in this region and it becomes in an important source of scattering. However, in the case  $n = 4$ , since the potential barrier is less important than the other cases (see in figure 2 the square and the inverted-triangle for  $n = 4$ ), the influence of the bulk monolayers becomes more important. Likewise, in this anomalous case, the reduced contribution of the interface scattering favours a diminishment of the total MR, that is reflected in figure 6.

The last measurements reported in [40] and extensive comparative studies of the growth, structure, magnetization and magnetotransport in Fe/Cr superlattices show that the intrinsic GMR originates from interfacial scattering and is determined by the interface width [31]. This experimental fact confirms the results shown in figure 7 and our earlier conclusion that the interface should be treated physically not as an ideal plane but as a transition zone between different materials where we can observe a mixture of two compounds (interdiffusion) and where not only a significant change of the potential but also a different kind of magnetism take place [6]. The DFT results [41] discussed in section 3.1 confirm the important role of the interface, specially the significant increase of magnetic moment at the interface for  $n = 5, 7$  (see figure 4). This fact finds its reflection in a significant change of the potential at the interface for different spin polarizations (figures 2 and 5). The difference in interface potential constitutes the main physical reason for different scattering of electrons with different spin orientation and it is the main mechanism responsible for GMR in multilayers.

#### 4. Conclusion

We have shown that using the two combined methods, the *ab initio* methodology for the accurate calculation of the potentials and the semiclassical approach based on the Fuchs–Sondheimer formalism, we obtain the GMR values for the trilayer Fe/Cr/Fe system which oscillates versus the thickness of the ferromagnetic layers. In literature, the GMR oscillations versus the nonmagnetic spacer are emphasized while the role of the ferromagnetic layer is considered sporadically. In the ordinary semiclassical approach the oscillations of this kind do not exist; however, our calculations can predict this oscillatory behaviour for ultrathin layers. Our results based on DFT calculations for the Fe/Cr system emphasize the very important role of the FLT via thickness dependent potential as well as the contribution of the interface to the GMR ratio. It is worthwhile to notice that the present approach does not contain any semiempirical parameter apart from the calibration constant  $c$ .

## Acknowledgments

The authors thank the CESGA supercomputer centre for access to supercomputers. One of us (MP) acknowledges partial support by the Xunta de Galicia, under project No PGIDIT02TMT20601PR.

## References

- [1] Baibich M N, Broto J M, Fert A, Nguyen Van Dau F, Petroff F, Etienne P, Creuzet G, Friederich A and Chazelas J 1988 *Phys. Rev. Lett.* **61** 2472
- [2] Bloemen P J H, Johnson M T, van de Vorst M T H, Coehoorn R, de Vries J J, Jungblut R, aan de Stegge J, Reinders A and de Jonge W J M 1994 *Phys. Rev. Lett.* **72** 764
- [3] Okuno S N and Inomata K 1994 *Phys. Rev. Lett.* **72** 1553
- [4] Edwards D M, Mathon J, Muniz R B and Phan M S 1991 *Phys. Rev. Lett.* **67** 493
- [5] Bruno P and Chappert C 1991 *Phys. Rev. Lett.* **67** 1602  
Bruno P and Chappert C 1991 *Phys. Rev. Lett.* **67** 2592
- [6] Wiatrowski G, Baldomir D, Warda K, Pereiro M, Wojtczak L and Arias J E 2004 *J. Magn. Magn. Mater.* **277** 285
- [7] Zahn P, Binder J, Mertig I, Zeller R and Dederichs P H 1998 *Phys. Rev. Lett.* **80** 4309
- [8] Hood R Q and Falicov L M 1992 *Phys. Rev. B* **46** 8287
- [9] Hood R Q, Falicov L M and Penn D R 1994 *Phys. Rev. B* **49** 368
- [10] Zahn P, Papanikolaou N, Erler F and Mertig I 2002 *Phys. Rev. B* **65** 134432
- [11] Vosko S H, Wilk L and Nusair M 1980 *Can. J. Phys.* **58** 1200
- [12] Herper H C, Szunyogh L, Entel P and Weinberger P 2003 *Phys. Rev. B* **68** 134421
- [13] Kohn W and Sham L J 1965 *Phys. Rev.* **140** A1133
- [14] Cherepin V T, Ostroukhov A A and Tomilenko V N 1986 *Poverkhnost' (Surface)* **6** 43
- [15] Weinert M 1981 *J. Math. Phys.* **22** 2433
- [16] Qian X and Hubner W 2003 *Phys. Rev. B* **67** 184414
- [17] Ortega J E, Himpfel F J, Mankey G J and Willis R F 1993 *Phys. Rev. B* **47** 1540
- [18] Mirbt S, Johansson B and Skriver H L 1996 *Phys. Rev. B* **53** R13310
- [19] Pérez-Díaz J L and Muñoz M C 1996 *Phys. Rev. B* **53** 13583
- [20] Visscher P B and Zhang H 1993 *Phys. Rev. B* **48** 6672
- [21] Johnson P D, Garrison K, Dong Q, Smith N V, Li D, Mattson J, Pearson J and Bader S D 1994 *Phys. Rev. B* **50** R8954
- [22] Camley R E and Barnas J 1988 *Phys. Rev. Lett.* **63** 664
- [23] Barnas J, Fuss A, Camley R E, Grünberg P and Zinn W 1990 *Phys. Rev. B* **42** 8110
- [24] Warda K, Wojtczak L, Baldomir D and Pereiro M 2001 *Surf. Rev. Lett.* **8** 271
- [25] Ziese M and Thornton M J 2001 *Spin Electronics* (Berlin: Springer)
- [26] Fuchs K 1938 *Proc. Camb. Phil. Soc.* **34** 100
- [27] Sondheimer E H 1952 *Adv. Phys.* **1** 1
- [28] Kubler J 2000 *Theory of Itinerant Electron Magnetism* (Oxford: Clarendon)
- [29] Man'kovsky S V, Baldomir D and Pereiro M 2003 *Int. J. Quantum Chem.* **91** 234
- [30] Warda K, Wojtczak L, Wiatrowski G, Baldomir D, Pereiro M and Arias J E 2002 *Czech. J. Phys.* **52** A157
- [31] Pereiro M, Botana J, Baldomir D, Warda K, Wojtczak L, Man'kovsky S, Iglesias M, Pardo V and Arias J E 2005 *J. Magn. Magn. Mater.* **290/291** 392
- [32] Gijs M A M, Lenczowski S K J and Giesbers J B 1993 *Phys. Rev. Lett.* **70** 3343
- [33] Schep K M, Kelly P J and Bauer G E W 1998 *Phys. Rev. B* **57** 8907
- [34] Fullerton E E, Kelly D M, Guimpel J and Schuller I K 1998 *J. Magn. Magn. Mater.* **184** 275
- [35] Colino J M, Schuller I K, Korenivski V and Rao K V 1996 *Phys. Rev. B* **54** 13030
- [36] Velez M and Schuller I K 1998 *J. Magn. Magn. Mater.* **184** 275
- [37] Mattson J E, Brubaker M E, Sowers C H, Conover M, Qiu Z and Bader S D 1991 *Phys. Rev. B* **44** 9378
- [38] Qiu Z Q, Mattson J E, Sowers C H, Welp U, Bader S D, Tang H and Walker J C 1992 *Phys. Rev. B* **45** 2252
- [39] Parkin S S P 1993 *Phys. Rev. Lett.* **71** 1641
- [40] Santamaria J, Gomez M-E, Cyrille M-C, Leighton C, Krishnan K K and Schuller I K 2001 *Phys. Rev. B* **65** 012412
- [41] Pereiro M, Baldomir D, Mankovsky S and Arias J 2003 *Int. J. Quantum Chem.* **91** 245